Sliding Friction of Amorphous Asperities on Crystalline Substrates: Scaling with Contact Radius and Substrate Thickness

Joseph M. Monti[*,†] and Mark O. Robbins[†,‡]

†*Department of Physics and Astronomy, Johns Hopkins University, Baltimore, MD 21218*

‡*Deceased 13 August 2020.*

E-mail: jmonti3@jhu.edu

Abstract

Disorder in the contact between an amorphous slider and a crystalline substrate leads to a cancellation of lateral forces. Atomically flat, rigid surfaces exhibit structural superlubricity, with the frictional stress in circular contacts of radius a vanishing as $1/a$. The inclusion of elasticity allows relative motion of domains on the surface in response to the random interfacial forces. The competition between disorder and elastic deformation is predicted to limit structural suberlubricity and produce a constant frictional stress for a larger than a characteristic domain size λ that depends on the ratio of the shear modulus G to the magnitude of interfacial shear stresses τ_0. Extensive simulations of a flat, amorphous punch sliding on a crystalline substrate with different system sizes and G/τ_0 are used to test scaling predictions and determine unknown prefactors that are needed for quantitative analysis. For bulk systems, we find an exponential decrease of the large a frictional stress and $1/\lambda$ with increasing G/τ_0. For thin free-standing films, the stress and $1/\lambda$ are inversely proportional to G/τ_0. These results

may help explain the size-dependent friction of nanoparticles and plate-like materials used as solid lubricants.

Keywords

nanotribology; structural superlubricity; amorphous nanoparticles; shear stress; solid lubricants

Amontons' macroscopic laws of friction state that the friction force is proportional to the load pushing surfaces together and independent of the total area where they overlap.[1] However, these laws are commonly explained by noting that surfaces only interact over a much smaller area of direct molecular contact A. If A is proportional to load and there is a constant shear stress τ in contacting regions, one recovers Amontons' laws.[1] To lower friction, one can use stiffer solids to lower A or find interfaces that minimize τ.

Nanoscale studies reveal an exciting phenomenon called structural superlubricity where τ actually vanishes as the radius a of contacting regions increases.[2–13] Indeed, theoretical arguments[2–5] predict that the shear stress at the interface between rigid, atomically flat surfaces should usually vanish at least as rapidly as $1/a$. Except in the rare case where the surfaces share a common period, the lateral forces that give rise to friction systematically or stochastically cancel. Even identical crystal surfaces slide without friction if they are rotated out of alignment. This surprising behavior has been observed in a range of experiments and simulations of individual contacts using both crystalline and amorphous surfaces.[2–14] However, these studies have considered contact radii below 100 nm and there is evidence that the key assumption of rigidity breaks down at large scales.

Scaling theories[15–21] and studies of single contacts between crystals[22–27] show that substrate elasticity introduces an elastic coherence length λ that is analogous to the Larkin

length in charge density wave conduction[28] or flux lattices in type-II superconductors[29] or raindrops on window panes.[30] Elasticity is irrelevant for lateral distances less than λ, but above this scale the system can deform in response to the interfacial potential. If a is larger than λ, the lateral forces between surfaces no longer cancel and τ saturates at a constant value for large a. Even for smaller a, analogous arguments predict pinning of macroscopic surfaces by deformation at scales larger than the asperity spacing.[15,16,31]

For crystal surfaces, λ is related to the core size b_{core} of a dislocation that accommodates the mismatch between the periods of the surfaces, allowing them to lock in local registry.[22–26] Simulations for a range of systems[25,26] showed τ saturated for $a > b_{core}$. Moreover, dislocations lowered the shear stress between identical aligned crystals, because parts of the interface could advance independently. As a result the constant τ at large scales was surprisingly insensitive to alignment and could be related to the Peierls stress for dislocation motion.

To our knowledge, experiments have not seen τ saturate for large crystalline surfaces, but recent experiments[32] of flat, amorphous antimony nanoparticles on a crystalline MoS_2 substrate found that τ saturated when the radius of the nanoparticles exceeded ~ 70 nm. Indeed, the nanoparticles underwent plastic deformation prior to sliding, implying that τ exceeded the yield stress of the nanoparticles. No saturation was observed for the same particles on graphite substrates.

In this paper we use simulations to study amorphous nanoparticles or asperities sliding over a crystalline substrate and determine how τ scales with a, the shear modulus G, and the magnitude of local shear stresses on individual atoms τ_0. For small radii, stiff substrates, and small τ_0, $\tau \propto 1/a$ as expected for structural superlubricity. The stress saturates when a exceeds a scale λ that rises exponentially with G/τ_0. Although this length comes from different arguments than the crystal-on-crystal case, the numerical values of τ/τ_0 have the same exponential scaling and similar values for amorphous and crystalline surfaces.

There has been great interest in friction of thin solid layers of graphene or MoS_2 as

realizations of nearly two dimensional (2D) behavior and as practical replacements for liquid lubricants.[1,13,31,33–37] We show that the scaling of λ and τ/τ_0 is different for amorphous asperities on such thin systems and that friction decreases with increasing film thickness h. Experiments have observed a similar trend for free-standing films of different h and we discuss how our results relate to past explanations.[33–35]

RESULTS AND DISCUSSION

Scaling of interfacial and substrate energies

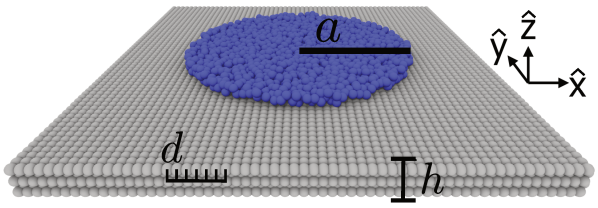

Figure 1: A flat, amorphous slider with radius $a \approx 17.8d$ in contact with a thin (quasi-2D) crystalline substrate with lattice constant d. The thickness of the substrate is h.

We consider an amorphous slider with a flat tip of radius a moving over the (001) surface of an fcc crystal with nearest-neighbor spacing d. A subsection of such a system is shown in Fig. 1.[38] As the slider moves, the disordered interfacial potential gives rise to a lateral force $\mathbf{f}$ on each substrate atom that varies with time and samples all directions. The root mean squared (rms) force on atoms in the sliding direction $\hat{x}$ at any instant can be used to define a characteristic local frictional shear stress on the surface $\tau_0 \equiv \sqrt{\langle |f_x|^2 \rangle}/d^2$. The simulation configuration we use differs from the prototypical sphere-on-flat geometry found in atomic force microscope (AFM) studies, but using a tip with a flat profile simplifies the system because the contact area is independent of pressure. In addition, the local shear stress under a flat tip does not systematically vary with the distance from the center of the contact, as it does for sphere-on-flat systems.[26]

For a rigid substrate, the forces from different regions add incoherently. The friction force

grows as $\tau_0 d^2$ times the square root of the number of contacting atoms $N \sim \pi a^2/d^2$. The static friction stress τ_{fric} is defined as the maximum force per area that must be overcome to allow sliding.[1] In the rigid limit this scales as $\tau_{rig} \equiv \tau_0/\sqrt{N} = \tau_0 d/\sqrt{\pi} a$. The force changes when the surface moves laterally by $\sim d$. Thus static friction can be associated with the system being trapped in an energy minimum per unit contact area that scales as $u_{int} \sim d\tau_{rig} \sim \tau_0 d^2/\sqrt{\pi} a$.

Different regions of the contact area will minimize their energy at different relative positions between tip and substrate. If the materials are elastic, it may become favorable to deform the surface on scales of order λ so that different regions can optimize their registry. As noted above, the displacements need only be of order d and the energy gain per unit area is of order $u_{int} \sim \tau_0 d^2/\lambda$. To calculate the elastic cost we use the fact that contact between two elastic solids can be mapped to contact between a rigid surface and an elastic substrate with an effective shear modulus G obtained by adding the compliances of the two solids in parallel (Methods).[39] Saint-Venant's principle says that a surface displacement of wavelength λ only penetrates into the substrate by $\sim \lambda$. Then, an elastic strain of order d/λ penetrating to a depth λ gives an elastic cost per unit area of $u_{el} \sim \lambda G (d/\lambda)^2 \sim G d^2/\lambda$. For quasi-2D films whose thickness h is smaller than λ, the deformation only penetrates to h and $u_{el} \sim h G (d/\lambda)^2$.

Following Imry and Ma[40] the Larkin length is given by the length where interfacial and elastic energies per unit area are comparable. From the above results for 2D systems, elasticity allows deformations above a Larkin length $\lambda \sim hG/\tau_0$ and the typical shear strength at large scales is $\tau_{fric} \sim \tau_0 d/\sqrt{\pi}\lambda \sim d\tau_0^2/hG$. A 2D interface between bulk elastic solids is considered the marginal dimensionality,[15] because interfacial and elastic terms scale in the same way with λ and always have ratio $u_{int}/u_{el} = G/\tau_0$. For G/τ_0 of order unity and smaller, disorder wins, and the system deforms. More careful analysis of higher order effects[15–18] shows that disorder wins even for stiffer systems beyond a Larkin length λ that grows exponentially with G/τ_0. The corresponding friction stress decreases exponentially

with G/τ_0. While several papers have discussed this exponential scaling, it has been difficult to test directly in simulations or to determine the prefactors needed to apply results to real systems.[15–18,20] The next two sections provide quantitative results for both 3D and 2D systems.

3D ELASTIC SUBSTRATE

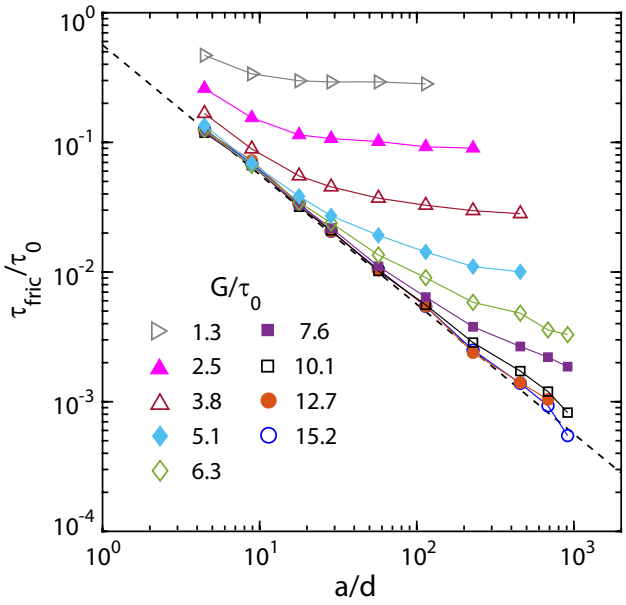

Figure 2: Static friction stress *versus* contact radius for 3D substrates and values of G/τ_0 shown in the legend. A dashed line indicates the analytic prediction for the rigid limit $\tau_{rig}/\tau_0 = d/\sqrt{\pi}a$. For $a < \lambda$ contacts exhibit structural superlubricity and follow the rigid prediction. For small G/τ_0, the stress then saturates at τ^{∞}_{fric} for $a > \lambda$. This regime is not accessible for large G/τ_0. Statistical errors are no larger than the symbol size.

Figure 2 shows the scaling of τ_{fric}/τ_0 with a/d for 3D systems of different stiffness. These results were obtained for a specific strength of the disordered potential, but results for other τ_0 show the same behavior. The stiffest systems exhibit structural superlubricity, $\tau_{fric} \approx \tau_{rig}$, over the accessible range of a. As G/τ_0 decreases, deviations from τ_{rig} set in at smaller a/d and τ_{fric}/τ_0 saturates at larger values. Direct examination of the local atomic displacements confirms that atoms move coherently when $\tau_{fric} \sim \tau_{rig}$. In contrast, independent motion becomes significant in larger contacts where $\tau_{fric} \sim \tau^{\infty}_{fric}$, as expected for $a > \lambda$. For contacts

with $a > \lambda$, the instantaneous friction stress during sliding is reduced when portions of the interface slip relative to the motion of the tip; see Supporting Information (SI) for movies that illustrate this behavior for large contacts.

Slip events may preferentially nucleate at the contact edge for punch-like geometries as a result of the stress concentration there.[39] However, elastic energy necessary for the slip process also accumulates near the strongest pinning sites, which may be located at any position in the contact region. This differs from the situation expected for a spherical tip, where the local shear strength depends on both the local shear stress $\sim \tau_0$ and the local pressure. Consequently, pinning of a disordered, spherical tip is most probable to occur near the center of the contact, where the pressure is highest.

In the very smallest ($a/d \approx 5$) and least stiff contacts, τ_{fric} is noticeably higher than τ_{rig}. Examining local forces showed that the total force was dominated by a few sites, making it easier to find favorable pinning sites and causing a deviation from $\sqrt{N}$ scaling.

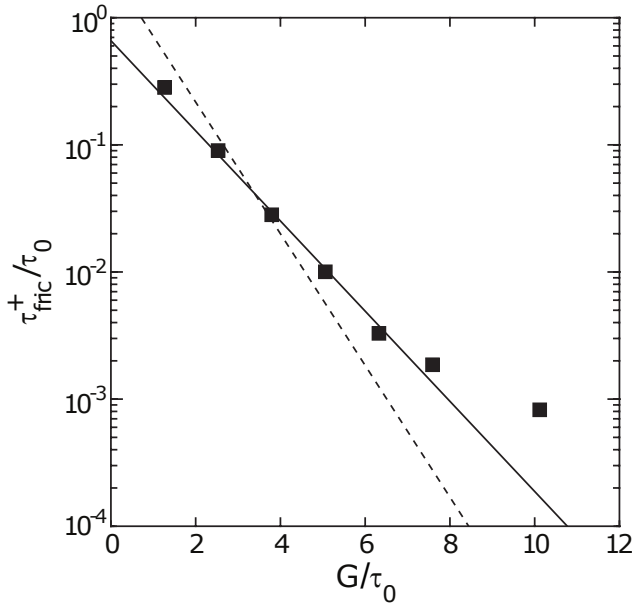

Figure 3: Static friction stress for the largest contact radius simulated at each value of G/τ_0 (Fig. 2). Statistical errors are comparable to the symbol size, but points represent an upper bound for τ^{∞}_{fric} because a is finite. A solid line indicates the prediction $\tau^{\infty}_{fric} \sim \tau^{+}_{fric}$ from Eq. 2 with $c_3 = 0.66$ and $c_2 = 0.82$. The dashed line is the rescaled Peierls stress of a single edge dislocation reported by Sharp *et. al.*:[25] $c_3 = 0.40$, $c_2 = 1.17$.

The Larkin length and limiting friction stress in large contacts are expected to scale as:[15,17,18,20,21]

$$\lambda/d = c_1 \exp[c_2 G/\tau_0] \quad , \tag{1}$$

$$\tau^{\infty}_{fric}/\tau_0 = c_3 c_1 d/\lambda = c_3 \exp[-c_2 G/\tau_0] \quad , \tag{2}$$

where the c_i are unknown constants. There may be corrections to this scaling for small G/τ_0 where λ approaches the lattice size and local shear forces may be large enough to produce a nonlinear response.

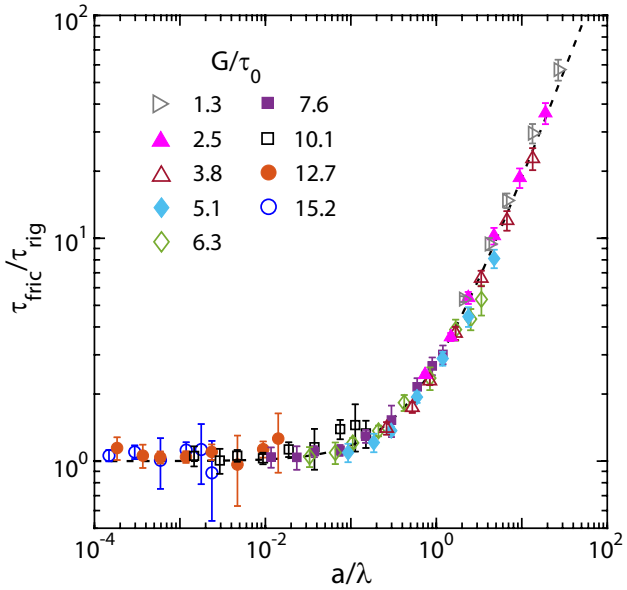

Figure 4: Static friction stress normalized by rigid limit as a function of a/λ for $c_2 = 0.82$, $c_1 = 1/c_3 = 1.5$, and values of G/τ_0 indicated in the legend. In the large contact limit, τ_{fric}/τ_{rig} grows linearly with contact radius. The dashed line shows data fit a simple interpolation between small and large a limits, $1 + \sqrt{\pi}a/\lambda$. Error bars are indicated when they are larger than the symbol size. Results for $a/d \approx 5$ are not included because lattice effects cause them to lie to the left of other points by about twice the symbol width.

Figure 3 shows the stiffness dependence of τ^{+}_{fric}, the shear stress in the largest contacts studied at each G/τ_0 (Fig. 2). For small G/τ_0 we reached the limiting large a behavior. For larger G/τ_0, τ_{fric} was still decreasing at the largest a and these points represent an upper bound for τ^{∞}_{fric}. To obtain information for larger G/τ_0 we performed a scaling collapse. The

data in Fig. 2 are replotted in Fig. 4 with τ_{fric} rescaled by τ_{rig} and a by λ from Eq. 1. The best collapse of data in the crossover between rigid and elastic limits was obtained using $c_2 = 0.82 \pm 0.05$. Changing c_1 just shifts all curves without affecting the collapse. We chose $c_1 = 1/c_3$ so that Eq. 2 simplifies to $\tau^{\infty}_{fric}/\tau_0 = d/\lambda$.

To determine c_3 and thereby c_1, we assumed that $\tau^{+}_{fric} \sim \tau^{\infty}_{fric}$ for $G/\tau_0 \leq 6.3$. Using $c_2 = 0.82$ from the scaling collapse in Fig. 4, we fit Eq. 2 to the data in this range of G/τ_0 in Fig. 3 (solid line), giving $c_3 = 0.66$, and fixing the value of $c_1 = 1.5$. With this choice of c_1, the friction exceeds the rigid limit by more than a factor of two at $a = \lambda$ in Fig. 4, and for large contacts $\tau_{fric}/\tau_{rig} = \sqrt{\pi}a/\lambda$. Figure 4 shows that the entire curve is fit by the simple interpolation between rigid and elastic limits $\tau_{fric}/\tau_{rig} = 1 + \sqrt{\pi}a/\lambda$ (dashed line).

The systematic uncertainties in these constants is hard to measure because of the limited range of G/τ_0 and the possibility of changes in scaling at small G/τ_0. Nonetheless, these results confirm the predicted scaling behavior while providing quantitative values for unknown prefactors. Note that because the strength of the interaction potential τ_0 only enters Eqs. 1-2 in the dimensionless ratio G/τ_0, our results are expected to hold for other potentials as well, provided that the range of G is adjusted accordingly.

The 3D estimates for τ^{∞}_{fric} are strikingly similar in magnitude and scaling to those for crystalline surfaces.[25] For both commensurate and incommensurate crystals, τ^{∞}_{fric} dropped exponentially with stiffness and was the same order of magnitude as the Peierls stress for moving an edge dislocation $\tau_{Peierls}$. The dashed line in Fig. 3 replots $\tau_{Peierls}$ from Fig. 3 of Ref. 25 using the rms lateral stress instead of the maximum ($\tau_0 = \tau_{max}/\sqrt{2}$). The results overlap at intermediate G/τ_0 and the prefactor c_2 for the exponential decay is about 40% larger than for the amorphous case studied here. Ref. 25 considered dislocations separating regions that were locked into perfect registry. For large G/τ_0, local regions of incommensurate surfaces may lock into a higher order commensurate state. The dislocations between these regions will have a finite but much lower $\tau_{Peierls}$ as observed for some rotation angles in Ref. 25 and in Ref. 41. This may lead to larger values of c_2 and much weaker pinning. The

degree of commensurability may also be a function of film thickness, with single layers being stretched or compressed into epitaxy, while thicker clusters retain the bulk lattice constant and exhibit superlubricity.[42]

The similarity in the stiffness-dependence of τ_{fric}^{∞} for amorphous and crystalline systems is in sharp contrast to the different scaling of λ and b_{core} in 3D. The latter rises only linearly with G/τ_0 instead of exponentially. For many tribopairs the effective shear modulus is 10 GPa or larger, while interfacial interactions typically give rise to $\tau_0 < 1$ GPa. Materials-specific values of τ_0 are not captured by the generic interfacial potential we used in our simulations and thus we are unable to provide precise values of τ_{fric}^{∞}. Nevertheless, the simplicity of Eq. 1 allows us to compute realistic values of λ. Assuming $G/\tau_0 = 10$ and $d = 0.3$ nm, Eq. 1 gives $\lambda \approx 2$ μm, compared to $b_{core} \approx 2.1$ nm. Thus it may be easier to achieve frictional pinning at the nanoscale with crystal-on-crystal contacts for bulk elastic solids.

2D ELASTIC SUBSTRATE

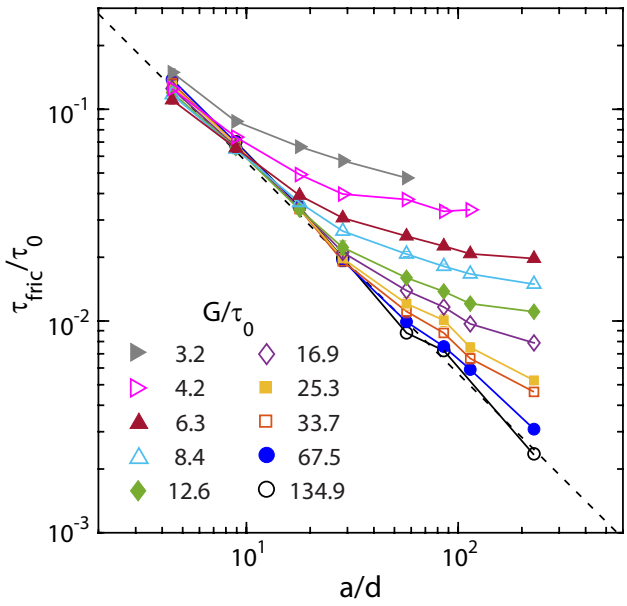

Figure 5: Static friction stress *versus* contact radius for fcc substrates with 3 layers and the indicated G/τ_0. Small, stiff systems follow the same superlubric scaling as 3D systems with $\tau_{fric} \approx \tau_{rig} = \tau_0 d/\sqrt{\pi} a$ (dashed line). As G decreases, results deviate from τ_{rig} at smaller a and τ_{fric}^{∞} increases.

This section presents results for a rigid amorphous disk sliding over a free-standing film of thickness h containing $n_l = \sqrt{2}h/d$ atomic layers. Given the mapping described above,[39] this can be mapped to experiments with an elastic amorphous disk of height h on a thick elastic substrate.[32]

Figure 5 shows the scaling of τ_{fric}/τ_0 with a/d for different G/τ_0 and $n_l = 3$ atomic layers (Fig. 1). As for 3D, there is a transition from rigid scaling $\tau_{fric} \approx \tau_{rig} = \tau_0 d/\sqrt{\pi}a$ at small a to a plateau at large a. The rigid regime is identical for 2D and 3D systems because it only reflects interfacial interactions. Because 2D systems are easier to deform, the transition to a constant τ_{fric} occurs at much smaller radii in 2D systems than in 3D systems.

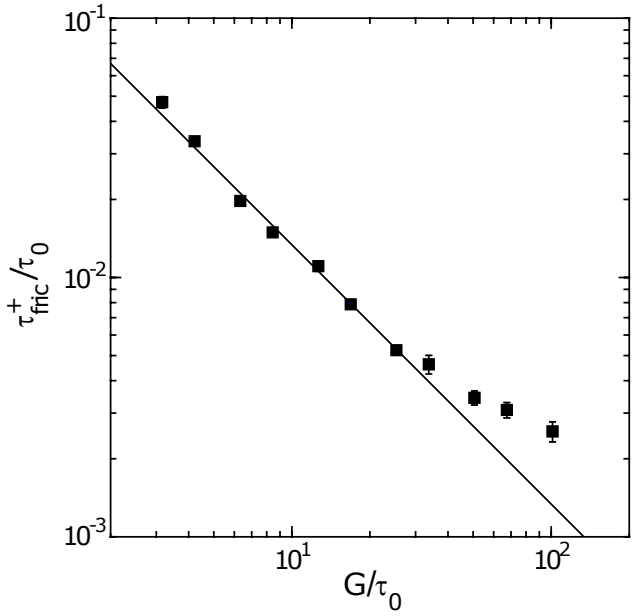

Figure 6: Static friction stress for the largest contact radius simulated at each value of G/τ_0 and $h/d = 3/\sqrt{2}$. Results for large G/τ_0 have not converged and represent an upper bound for τ^{∞}_{fric}. A solid line indicates the prediction $\tau^{\infty}_{fric}/\tau_0 \sim \tau^{+}_{fric}/\tau_0 = c_5 d\tau_0/hG$ with $c_5 = 0.28$. Statistical errorbars are shown when they are larger than the symbol size.

Scaling arguments discussed above predict:

$$\lambda/d = c_4 hG/d\tau_0 \quad , \tag{3}$$

$$\tau^{\infty}_{fric}/\tau_0 = c_5 d\tau_0/hG \quad , \tag{4}$$

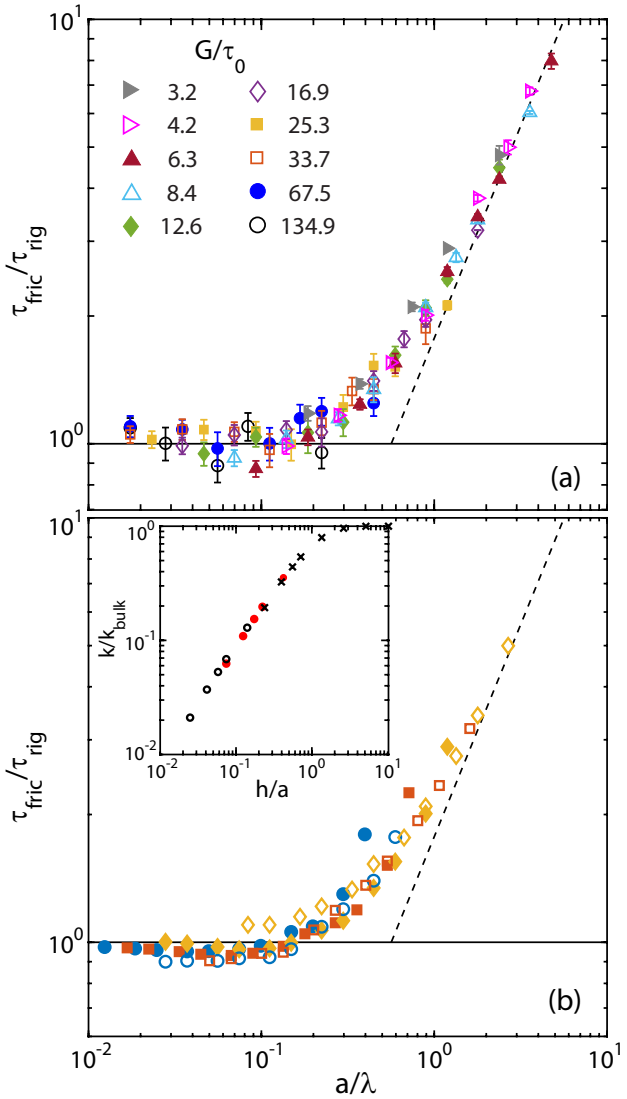

Figure 7: (a) Scaling plot of τ_{fric}/τ_{rig} against a/λ for the indicated G/τ_0. Results for different stiffness collapse with $\lambda/d = c_4 hG/d\tau_0$ and $c_4 = 1/c_5 \approx 3.6$. In the large contact limit, τ_{fric}/τ_{rig} grows linearly with contact radius (dashed line). (b) Similar collapse for films of 3 (diamonds), 5 (squares) and 9 (circles) layers and $a/d = 28.5$ (filled symbols) or 85.5 (open symbols). The inset shows that the stiffness characterizing elastic energy costs rises linearly with film thickness at small h/a and saturates at the bulk 3D value for $h/a \gg 1$. Results are for $a/d = 8.9$ (crosses), 28.5 (red circles) and 85.5 (open circles).

with unknown constants c_4 and c_5. Figure 6 shows the stress in the largest contacts studied as a function of G/τ_0. Again approximating τ_{fric}^{∞} by τ_{fric}^{+}, converged results follow the inverse relation of Eq. 4 with $c_5 = 0.28$. For $G/\tau_0 \gtrsim 30$ the stress was still significantly decreasing at the largest a studied.

Figure 7(a) shows the results from Fig. 5 with τ_{fric} rescaled by τ_{rig} and a rescaled by the Larkin length from Eq. 3. As in 3D, the collapse is independent of c_4 and we choose $c_4 = 1/c_5 \approx 3.6$ to give $\tau_{fric}/\tau_0 = d/\lambda$. The rescaled results follow rigid scaling for small a/λ and rise as $\sqrt{\pi}a/\lambda$ in large contacts. The crossover is slightly sharper than the simple interpolation formula used in 3D.

Implicit in our discussion is the assumption that a substrate with finite thickness may be treated as effectively 2D (quasi-2D). For a 3D substrate, rigidly displacing a circle of radius a produces a restoring force and elastic energy characterized by a stiffness[39] $k_{bulk} = 8Ga/(1+\nu)$, where ν is Poisson's ratio. The scaling arguments above assume that this stiffness is reduced by a factor of h/a when $h < a$. To confirm this we calculated the lateral stiffness k of films for different a and h. The inset to Fig. 7(b) shows that the ratio k/k_{bulk} is a universal function of h/a even for films of as few as 3 discrete layers. At small h the ratio obeys quasi-2D scaling and rises linearly with h/a. It saturates at unity for $h \gg a$.

These results for k indicate that Eq. 3 can be used to calculate λ for $h/a \lesssim 0.5$. Figure 7(b) confirms that results for 3, 5, and 9 layers at two values of a and a range of G/τ_0 collapse. The collapsed curve is consistent with that in panel (a) but the data are plotted separately for clarity. Note that the results in both panels seem to fall slightly below the rigid result for $a/\lambda \approx 0.1$ before rising. The source of this potential nonmonotonic behavior is unclear.

For $G/\tau_0 \approx 1$, the 3D and 2D expressions Eqs. 1 and 3 give similar numerical values of λ that are only a few times larger than d. Nonlinear effects may be important in this limit and estimates based on the yield stress suggest G/τ_0 will usually be larger. As an example, an estimate of λ for a 2D substrate with three lattice planes can be obtained by once again

assuming $G/\tau_0 = 10$ and $d = 0.3$ nm. Using Eq. 3 with these values gives $\lambda \approx 23$ nm, a value ~ 100 times smaller than we obtained earlier with the same parameters for a bulk elastic substrate.

Experimental studies[32] of amorphous Sb nanoparticles found a constant shear stress for $a \gtrsim 70$ nm on an MoS_2 substrate but superlubricity on a graphite substrate. The mapping of these experiments to our simulations is not exact because both substrates are highly anisotropic elastic materials and neither has atoms lying on a square lattice. However, equating the area per sulphur atom to d^2 gives $d = 0.29$ nm, $\lambda/d \sim 240$ and $G/\tau_0 = 6.2$ for 3D systems. In addition, the scaling with the number N of S atoms in the rigid limit[32] gives $\tau_0 \sim 450$ MPa, which is comparable to the stress (290 MPa) from density functional calculations.[32] Together these results would imply $G \sim 3$ GPa. The shear stress for Sb on graphite was about 4 times lower. Using the same G and d one finds $\lambda \sim 0.3$ m for Sb on graphite, and the corresponding τ_{fric}^{∞} would be immeasurably small.

The above estimate of G for Sb is relatively small. Adding the modulii of crystalline Sb (20 GPa[43]) and MoS_2 (~ 32 GPa[44]) in series[39] gives $G \sim 12$ GPa. However, amorphous solids can be an order of magnitude more compliant, depending on deposition conditions.[45,46] A low modulus would correlate with a low yield stress, explaining the observation of permanent plastic deformation in some nanoparticles.[32] It would be interesting to measure the shear modulus of Sb nanoparticles or attempt to increase G by annealing.[45] Another factor may be the thickness of the antimony particles $20 - 50$ nm, which was comparable to λ. This may reduce the stiffness from the 3D case and enhance friction.

Thin films of MoS_2 and graphite are frequently used as solid lubricants. Recent AFM experiments have revealed a steady decrease in friction as the number of layers in the film increases.[33,34] AFM contacts are generally small enough ($a/d < 10$) that they would be in the rigid limit if they were flat. However thin films can bend and pucker ahead of the tip. This increases the area of contact and adds new dissipation mechanisms that depend on the displacement.[33,34] Recent work shows that the experimental trends can be reproduced by

enriching the simple Prandtl-Tomlinson model with an extra degree of freedom that encodes deformation in the film.[37]

The results presented here extend contact and substrate sizes well beyond past simulations and AFM tip radii to scales that may be relevant for asperities on macroscopic surfaces.[1,13] The potential for bending and puckering was explicitly removed so that only in-plane displacements at the surface could produce friction.[33,34] Even in this limit there is a strong dependence of friction on thickness with $\tau_{fric}^{\infty} \sim 1/h$.

Solid lubricants are known to form transfer layers on rough surfaces.[1,13,47] Sliding then occurs between transfer layers on opposing surfaces which may have lower friction because of structural superlubricity between plates.[13] Stable transfer layers must have a larger friction with the substrate than the opposing surface. Our results suggest that elastic deformations may produce a high friction between thin plates and amorphous surfaces. Once locked in place, these plates would become part of a 3D elastic solid and friction with the opposing surface would be suppressed. This locking and the influence of multiscale roughness will be interesting topics for future investigation.

CONCLUSIONS

The results presented above verify scaling predictions for the stiffness-dependence of the Larkin length and the asymptotic frictional shear stress in contacts of amorphous solids with bulk elastic solids and thin free-standing films. For both substrate classes, structural superlubricity holds up to $a \sim \lambda$, and the frictional shear stress approaches a constant τ_{fric}^{∞} in larger contacts. The values of $1/\lambda$ and τ_{fric}^{∞} drop exponentially with G/τ_0 in 3D and linearly for thin films. Estimates of λ using realistic values of G/τ_0 and d showed that frictional pinning by disorder occurs more readily on 2D substrates than on 3D substrates at the nanoscale.

Our simulations showed that a crossover between 2D and 3D frictional behavior is ex-

pected when the thin film thickness approaches the contact radius. Variation of the film thickness for $h \ll a$ showed that h and G/τ_0 play analogous roles in determining the Larkin length in 2D. Our results demonstrate that the film thickness impacts the frictional shear stress even when only in-plane displacements are permitted. Therefore, film thickness can be used as independent control on the frictional response for fixed material parameters and contact size.

METHODS

A general relation allows contact between two elastic solids to be mapped to a rigid solid on an elastic substrate.[39] The elastic substrate was the (001) surface of an fcc crystal with nearest neighbor spacing d. A rigid amorphous disk of radius a was cut from a Lennard-Jones glass of density $\rho = 1.2d^{-3}$ prepared by rapidly quenching a liquid. The disk and substrate atoms interacted with a truncated Lennard-Jones potential with $\sigma = d/\sqrt[6]{2}$. The potential and forces were smoothed to zero from 1.2σ to 1.5σ.[48] The disk was thicker than the range of interactions.

Friction was measured by moving the slider across the substrate in discrete steps, minimizing the energy at each step. This is comparable to low sliding rate experiments where the probe speed is many orders of magnitude smaller than the sound speed in the solid. Error bars represent uncertainty in the average static friction stress value obtained by performing sliding for many realizations of amorphous disks with a given radius a.

Atomic displacements in the 3D substrate were treated using a Green's function method[49–51] that computes the exact linear response and is implemented in LAMMPS.[48] An isotropic Green's function with Poisson's ratio $\nu = 0.5$ was chosen to decouple normal and lateral forces from the disk. The friction only depends on lateral forces to leading order in this case and we set normal forces to zero so substrate atoms remained at a fixed height with a minimum separation of σ between crystal and amorphous atoms. This approach ensures

atoms feel the random lateral force assumed in scaling theories. Normal forces can only influence friction at small G/τ_0 where nonlinear effects become important.

2D simulations used the same random surface interactions. The substrate contained n_l crystal layers with harmonic springs k_b between nearest neigbors, yielding an effective shear modulus[52] $G = 0.468k_b/d$. In general, G will depend upon sliding direction for crystalline substrates. Free-standing films had a square geometry of length L with the periphery fixed in place to prevent translation. The friction was insensitive to L for $L \geq 8a$.

Acknowledgement

The authors thank T. Sharp for helpful conversations and R. Leheny for assistance with preparation of the final manuscript. This material is based upon work supported by the National Science Foundation under Grant No. DMR-1411144 and DMR-1929467. Simulations were performed at the Maryland Advanced Research Computing Center and the Homewood High-Performance Cluster.

Supporting Information Available

The Supporting Information is available free of charge *via* the Internet at http://pubs.acs.org.

Movie of cumulative substrate displacement in sliding direction; movie of frame-by-frame slip events; associated friction trace; description of parameters for movies.

References

(1) Bowden, F. P.; Tabor, D. *The Friction and Lubrication of Solids*; Clarendon Press: Oxford, 2001.

(2) Hirano, M.; Shinjo, K. Atomistic Locking and Friction. *Phys. Rev. B* **1990**, *41*, 11837–11851.

(3) Müser, M. H.; Wenning, L.; Robbins, M. O. Simple Microscopic Theory of Amontons's Laws for Static Friction. *Phys. Rev. Lett.* **2001**, *86*, 1295–1298.

(4) de Wijn, A. S. (In)commensurability, Scaling, and Multiplicity of Friction in Nanocrystals and Application to Gold Nanocrystals on Graphite. *Phys. Rev. B* **2012**, *86*, 085429.

(5) Dietzel, D.; Feldmann, M.; Schwarz, U. D.; Fuchs, H.; Schirmeisen, A. Scaling Laws of Structural Lubricity. *Phys. Rev. Lett.* **2013**, *111*, 235502.

(6) Krim, J.; Solina, D. H.; Chiarello, R. Nanotribology of a Kr Monolayer: A Quartz-Crystal Microbalance Study of Atomic-Scale Friction. *Phys. Rev. Lett.* **1991**, *66*, 181–184.

(7) Cieplak, M.; Smith, E. D.; Robbins, M. O. Molecular Origins of Friction: The Force on Adsorbed Layers. *Science* **1994**, *265*, 1209–1212.

(8) Müser, M. H.; Robbins, M. O. Conditions for Static Friction between Flat Crystalline Surfaces. *Phys. Rev. B* **2000**, *61*, 2335–2342.

(9) Wenning, L.; Müser, M. H. Friction Laws for Elastic Nano-Scale Contacts. *Europhys. Lett.* **2001**, *54*, 693–699.

(10) Dienwiebel, M.; Verhoeven, G. S.; Pradeep, N.; Frenken, J. W. M.; Heimberg, J. A.; Zandbergen, H. W. Superlubricity of Graphite. *Phys. Rev. Lett.* **2004**, *92*, 126101.

(11) Dietzel, D.; Ritter, C.; Mönninghoff, T.; Fuchs, H.; Schirmeisen, A.; Schwarz, U. D. Frictional Duality Observed during Nanoparticle Sliding. *Phys. Rev. Lett.* **2008**, *101*, 125505.

(12) Hirano, M.; Shinjo, K.; Kaneko, R.; Murata, Y. Anisotropy of Frictional Forces in Muscovite Mica. *Phys. Rev. Lett.* **1991**, *67*, 2642–2645.

(13) Martin, J. M.; Donnet, C.; Le Mogne, T.; Epicier, T. Superlubricity of Molybdenum Disulphide. *Phys. Rev. B* **1993**, *48*, 10583–10586.

(14) Deng, H.; Ma, M.; Song, Y.; He, Q.; Zheng, Q. Structural Superlubricity in Graphite Flakes Assembled under Ambient Conditions. *Nanoscale* **2018**, *10*, 14314–14320.

(15) Volmer, A.; Nattermann, T. Towards a Statistical Theory of Solid Dry Friction. *Z. Phys. B: Condens. Matter* **1997**, *104*, 363–371.

(16) Caroli, C.; Nozières, P. Hysteresis and Elastic Interactions of Microasperities in Dry Friction. *Eur. Phys. J. B* **1998**, *4*, 233–246.

(17) Müser, M. H.; Urbakh, M.; Robbins, M. O. *Adv. Chem. Phys.*; John Wiley & Sons, Ltd: Hoboken, 2003; Chapter 5, pp 187–272.

(18) Persson, B.; Tosatti, E. Theory of Friction: Elastic Coherence Length and Earthquake Dynamics. *Solid State Commun.* **1999**, *109*, 739–744.

(19) Sokoloff, J. B.; Tomassone, M. S. Effects of Surface Defects on Friction for a Thin Solid Film Sliding over a Solid Surface. *Phys. Rev. B* **1998**, *57*, 4888–4894.

(20) Sokoloff, J. B. Static Friction between Elastic Solids Due to Random Asperities. *Phys. Rev. Lett.* **2001**, *86*, 3312–3315.

(21) Müser, M. H. Structural Lubricity: Role of Dimension and Symmetry. *Europhys. Lett.* **2004**, *66*, 97–103.

(22) Hurtado, J. A.; Kim, K.-S. Scale Effects in Friction of Single-Asperity Contacts. I. From Concurrent Slip to Single-Dislocation-Assisted Slip. *Proc. Royal Soc. A* **1999**, *455*, 3363–3384.

(23) Hurtado, J. A.; K.-S.Kim, Scale Effects in Friction of Single-Asperity Contacts. II. Multiple-Dislocation-Cooperated Slip. *Proc. Royal Soc. A* **1999**, *455*, 3385–3400.

(24) Gao, Y. A Peierls Perspective on Mechanisms of Atomic Friction. *J. Mech. Phys. Solids* **2010**, *58*, 2023–2032.

(25) Sharp, T. A.; Pastewka, L.; Robbins, M. O. Elasticity Limits Structural Superlubricity in Large Contacts. *Phys. Rev. B* **2016**, *93*, 121402.

(26) Sharp, T. A.; Pastewka, L.; Lignères, V. L.; Robbins, M. O. Scale- and Load-Dependent Friction in Commensurate Sphere-on-Flat Contacts. *Phys. Rev. B* **2017**, *96*, 155436.

(27) Kim, W. K.; Falk, M. L. Atomic-Scale Simulations on the Sliding of Incommensurate Surfaces: The Breakdown of Superlubricity. *Phys. Rev. B* **2009**, *80*, 235428.

(28) Lee, P. A.; Rice, T. M. Electric Field Depinning of Charge Density Waves. *Phys. Rev. B* **1979**, *19*, 3970–3980.

(29) Larkin, A. I.; Ovchinnikov, Y. N. Pinning in Type II Superconductors. *J. Low Temp. Phys.* **1979**, *34*, 409–428.

(30) Robbins, M. O.; Joanny, J. F. Contact Angle Hysteresis on Random Surfaces. *Europhys. Lett.* **1987**, *3*, 729–735.

(31) Müser, M. H. Are There Limits to Superlubricity of Graphene in Hard, Rough Contacts? *Front. Mech. Eng.* **2019**, *5*, 28.

(32) Dietzel, D.; Brndiar, J.; Štich, I.; Schirmeisen, A. Limitations of Structural Superlubricity: Chemical Bonds *versus* Contact Size. *ACS Nano* **2017**, *11*, 7642–7647.

(33) Li, S.; Li, Q.; Carpick, R. W.; Gumbsch, P.; Liu, X. Z.; Ding, X.; Sun, J.; Li, J. The Evolving Quality of Frictional Contact with Graphene. *Nature* **2016**, *539*, 541–545.

(34) Lee, C.; Li, Q.; Kalb, W.; Liu, X.-Z.; Berger, H.; Carpick, R. W.; Hone, J. Frictional Characteristics of Atomically Thin Sheets. *Science* **2010**, *328*, 76–80.

(35) Curry, J. F.; Hinkle, A. R.; Babuska, T. F.; Wilson, M. A.; Dugger, M. T.; Krick, B. A.; Argibay, N.; Chandross, M. Atomistic Origins of Temperature-Dependent Shear Strength in 2D Materials. *ACS Appl. Nano Mater.* **2018**, *1*, 5401–5407.

(36) Ye, Z.; Martini, A. Atomistic Simulation of the Load Dependence of Nanoscale Friction on Suspended and Supported Graphene. *Langmuir* **2014**, *30*, 14707–14711.

(37) Andersson, D.; de Wijn, A. S. Understanding the Friction of Atomically Thin Layered Materials. *Nat. Comm.* **2020**, *11*, 420.

(38) Stukowski, A. Visualization and Analysis of Atomistic Simulation Data with OVITO-the Open Visualization Tool. *Modell. Simul. Mater. Sci. Eng.* **2010**, *18*.

(39) Johnson, K. L. *Contact Mechanics*; Cambridge University Press: Cambridge, 1985.

(40) Imry, Y.; Ma, S.-k. Random-Field Instability of the Ordered State of Continuous Symmetry. *Phys. Rev. Lett.* **1975**, *35*, 1399–1401.

(41) Mandelli, D.; Guerra, R.; Ouyang, W.; Urbakh, M.; Vanossi, A. Static Friction Boost in Edge-Driven Incommensurate Contacts. *Phys. Rev. Materials* **2018**, *2*, 046001.

(42) Guerra, R.; Tosatti, E.; Vanossi, A. Slider Thickness Promotes Lubricity: From 2D Islands to 3D Clusters. *Nanoscale* **2016**, *8*, 11108–11113.

(43) Poole, C. P. *Encyclopedic Dictionary of Condensed Matter Physics*; Academic Press: San Diego, 2004.

(44) Imani Yengejeh, S.; Liu, J.; Kazemi, S. A.; Wen, W.; Wang, Y. Effect of Structural Phases on Mechanical Properties of Molybdenum Disulfide. *ACS Omega* **2020**, *5*, 5994–6002.

(45) Hessinger, J.; White, B. E.; Pohl, R. O. Elastic Properties of Amorphous and Crystalline Ice Films. *Planet. Space Sci.* **1996**, *44*, 937–944.

(46) Schultrich, B.; Scheibe, H. J.; Grandremy, G.; Drescher, D.; Schneider, D. Elastic Modulus as a Measure of Diamond Likeness and Hardness of Amorphous Carbon Films. *Diamond Relat. Mater.* **1996**, *5*, 914–918.

(47) Wahl, K. J.; Belin, M.; Singer, I. L. A Triboscopic Investigation of the Wear and Friction of MoS2 in a Reciprocating Sliding Contact. *Wear* **1998**, *214*, 212–220.

(48) Plimpton, S. Fast Parallel Algorithms for Short-Range Molecular Dynamics. *J. Comput. Phys.* **1995**, *117*, 1 – 19.

(49) Hockney, R. Potential Calculation and Some Applications. *Methods Comput. Phys.* **1970**, *9*, 135–211.

(50) Campañá, C.; Müser, M. H. Practical Green's Function Approach to the Simulation of Elastic Semi-Infinite Solids. *Phys. Rev. B* **2006**, *74*, 075420.

(51) Pastewka, L.; Sharp, T. A.; Robbins, M. O. Seamless Elastic Boundaries for Atomistic Calculations. *Phys. Rev. B* **2012**, *86*, 075459.

(52) Luan, B.; Robbins, M. O. Contact of Single Asperities with Varying Adhesion: Comparing Continuum Mechanics to Atomistic Simulations. *Phys. Rev. E* **2006**, *74*, 026111.